


Back-to-back Schottky junction photodetectors based on CVD grown CsPbBr_3 microcrystalline striped films ^{EP}

Cite as: AIP Advances **9**, 125039 (2019); <https://doi.org/10.1063/1.5114664>

Submitted: 24 June 2019 . Accepted: 06 December 2019 . Published Online: 24 December 2019

Di Cui, Cancan Tian, Yunpeng Wang , Fei Wang, Zhe Yang, Jingjing Mei, Hongzhen Liu, and Dongxu Zhao

COLLECTIONS

 This paper was selected as an Editor's Pick



View Online



Export Citation



CrossMark

AIP Conference Proceedings
FLASH WINTER SALE!

50% OFF ALL PRINT PROCEEDINGS

ENTER CODE 50DEC19 AT CHECKOUT



Back-to-back Schottky junction photodetectors based on CVD grown CsPbBr_3 microcrystalline striped films

Cite as: AIP Advances 9, 125039 (2019); doi: 10.1063/1.5114664

Submitted: 24 June 2019 • Accepted: 6 December 2019 •

Published Online: 24 December 2019



Di Cui,^{1,2} Cancan Tian,^{1,2} Yunpeng Wang,^{1,a)}  Fei Wang,¹ Zhe Yang,^{1,2} Jingjing Mei,^{1,2} Hongzhen Liu,^{1,2} and Dongxu Zhao¹

AFFILIATIONS

¹State Key Laboratory of Luminescence and Applications, Changchun Institute of Optics, Fine Mechanics and Physics, Chinese Academy of Sciences, 3888 Dongnanhu Road, Changchun 130021, People's Republic of China

²University of Chinese Academy of Sciences, Beijing 100049, People's Republic of China

^{a)}Author to whom correspondence should be addressed: wangyunpeng@cimop.ac.cn. Tel.: 0431-86708227.

ABSTRACT

In recent years, a new type of lead halide perovskite has attracted a lot of attention for next-generation photodetectors (PDs) with high responsivity, good detectivity, and fast photoresponse speed. Specifically, cesium based all-organic perovskites exhibit better photostability and therefore have achieved increasing success in PDs recently. For reducing the leak current and increasing the response speed of photoconductive PDs, back-to-back Schottky junction PD is designed and fabricated through a direct growth approach of CsPbBr_3 microcrystal (MC) films on indium tin oxide (ITO) electrodes by the chemical vapor deposition (CVD) method. Due to the enhanced Schottky barrier height and threshold voltage between CsPbBr_3 and ITO electrodes, the PD exhibits the on/off ratio of up to 10^4 , peak responsivity of 3.9 AW^{-1} , detectivity of 3.8×10^{12} , and fast response speed of 0.22 ms (rise time) and 0.45 ms (decay time). In addition, the stability of PD is also enhanced by the high crystal quality of CVD grown CsPbBr_3 MCs.

© 2019 Author(s). All article content, except where otherwise noted, is licensed under a Creative Commons Attribution (CC BY) license (<http://creativecommons.org/licenses/by/4.0/>). <https://doi.org/10.1063/1.5114664>

Because of their small size, light weight, good linearity, and sensibility, photodetectors (PDs) made of different semiconductor materials have been widely used in various fields such as imaging, environmental monitoring, chemical/biological sensing, optical communication, and so on.^{1–5} In order to meet the requirements of optical information collection in newly developed applications, such as face and object identification in secure or self-driving systems, the development of a new type of material for high performance PDs is required. Lead halide perovskites with the structure of ABX_3 ($\text{A} = \text{CH}_3\text{NH}_3^+$ or Cs^+ ; $\text{B} = \text{Pb}^{2+}$, $\text{X} = \text{Cl}^-$, Br^- , or I^-) have recently shown great potential applications in laser,^{6,7} light emitting diodes (LEDs),^{8–11} PDs,^{12–14} and especially solar cells^{15–17} due to their outstanding optoelectronic properties, including high mobility, long diffusion length, ultrafast charge generation, easy preparation, etc. Compared with organometal halide perovskites with CH_3NH_3^+ or other organic cations as A-site elements, cesium based all-inorganic perovskites exhibit better photostability.^{18,19} Therefore,

the polycrystalline films^{20–23} and single crystals^{24,25} of CsPbBr_3 were widely investigated, and great progress has been achieved in the field of PDs recently. In 2016, Zeng *et al.* fabricated the CsPbBr_3 films via the centrifugal-casting method; after applying interdigitated Au as electrodes, the PD with the responsivity of 10.04 mAW^{-1} and the detectivity of 10^8 was achieved.²⁶ Wu *et al.* synthesized high-quality CsPbBr_3 single crystals via the inverse temperature crystallization method, and the assembled PDs showed the detectivity of 10^{11} and the response time of 230 ms in 2017.²⁴ In the past years, the photoconductive PDs based on the different morphology of CsPbBr_3 such as nanocrystals (NCs),^{27,28} microcrystals (MCs),^{29,30} nanowires,²⁰ and nanoplates²² were constructed. Meanwhile, PDs with different electrodes, such as Au,^{23,26,27} Pt,²⁴ ITO,^{21,29} and graphite,³⁰ were also investigated.

Compared with photoconductive devices, the inner energy barrier formed at p-n or p-i-n junctions of photovoltaic detectors could effectively lower the dark current and accelerate the photoresponse

speed.^{12,31} Similarly, the Schottky contact between the metal electrode and semiconductor could also bring in energy barrier and then realize rectifying behavior at the M-S junction. The detectors with back-to-back Schottky junctions have been widely constructed and investigated on metal oxide semiconductors and carbon nanotubes, and the enhanced sensitivity and increased response speed were also achieved.^{32–35} Therefore, it is a facile way to realize high performance PDs with flexible and simple manufacturing processes. In 2016, Bakr *et al.* reported the formation of the Schottky junction at the interface between Pt and $\text{CH}_3\text{NH}_3\text{PbBr}_3$ single crystals, and the detectivity of 10^{10} Jones was achieved.³⁶ Recently, Wu *et al.* fabricated a high performance resistive switching device on the basis of the Schottky junction at the perovskite/ITO interface, and the calculated Schottky barrier height was 0.3 eV.³⁷ Fang *et al.* reported that the dark current of the device can be effectively reduced by the Schottky barrier between CsPbBr_3 microwire and indium tin oxide (ITO), and the detectivity of 10^{12} Jones and the on/off ratio of more than 2 orders of magnitude were obtained.³⁸ However, the threshold voltage of the reported perovskite Schottky PDs is all around 2 V,^{36–38} and the reported barrier height of the Schottky junction is 0.3 V,³⁷ which is much lower than the Schottky-Mott model defined value. This is because perovskite materials are usually fabricated by the solution-processed method, which have brought abundant residual solvent molecules and surface groups into perovskites. The undesired compound and interface states between the electrode and perovskites tend to pin the center of the bandgap to the Fermi level, which is called the Fermi level pinning effect;^{32,35} then reduce the Schottky barrier height; and diminish the performance of the devices.

In this work, we demonstrate a direct growth approach of CsPbBr_3 MC films on interdigital (IDL) patterned ITO electrodes by the chemical vapor deposition (CVD) method. The CVD method, which allows the chemical reagents of the film deposition process to react on the surface of a substrate in vapor phase, is widely used for the growth of compound crystal films in industry today. By varying the experimental conditions of CVD such as growth temperature, reaction gas mixture, and gas flows, the physical, tribological, and chemical properties of materials can be adjusted more easily than by the PVD (physical vapor deposition) method. Compared to the solution method, the sealed and solvent free environment of the CVD technique during the growth process could avoid the grain boundary, surface defects, and groups, which could effectively enhance the carrier transport characteristic and chemical stability of thin films.³⁹ As a result, the interface defects between the perovskite and electrode could be reduced and consequently a contact with better electrical properties could be obtained. The CVD growth of perovskite can effectively avoid the solvent molecules and surface groups introduced during the wet chemical synthesis procedure, then increase the Schottky barrier height, and improve the performance of the device. Back-to-back dual-Schottky PDs are designed and fabricated through the direct CVD growth process, which will provide a low-cost and simplified strategy for high-performance visible-light PDs.

In this work, all-inorganic CsPbBr_3 striped films were synthesized on IDL ITO electrodes by the CVD method. As shown in Fig. 1(a), the reactants were prepared by mixing CsBr (99.9%) with PbBr_2 (99.0%) in 1:1M ratio and grinding them thoroughly. Then, the reactants were into an alumina boat. The laser etched

IDL ITO substrates with a line width of 50 μm were located downstream of the source boat with a distance of 12 cm. Before heating, the pressure of the chamber was pumped down to 180 Pa. Then, the temperature of the source boat was raised to 610 $^\circ\text{C}$ at the rate of 20 $^\circ\text{C min}^{-1}$ with 100 sccm Ar (99.999%) flow. After 20 min of reaction, the furnace was naturally cooled to room temperature. The perovskites tend to follow the Volmer-Weber island formation heteroepitaxial growth mode, and the surface adhesive force plays an important role in the growth process. At the beginning of the growth process, the atoms are primarily absorbed on the rough side edge of ITO IDT electrodes. Then, CsPbX_3 were grown along the side and full fill the gaps between IDT fingers. With the optimized growth time, the film would not cover the whole ITO and glass surface. During the growth procedure of CsPbBr_3 films, no mask was used. The yellow product grown on the substrates was CsPbBr_3 materials.

It is well known that introducing block layers or energy barriers is the most direct way to reduce the leak current and quicken the response speed of PDs. Figure 1(b) shows the structure illustration of our device. The main problem of our work is whether Schottky junctions could be formed at the CsPbBr_3 /ITO interface. In Fig. 1(c), the field emission scan electron microscopy (FE-SEM) image of the as-grown sample indicates that the CsPbBr_3 striped films are successfully grown in the gaps among ITO patterns with 50 μm widths. The striped films are constituted by several micro-sized crystals of CsPbBr_3 , as shown in Fig. 1(d). In Fig. S1 (supplementary material), the cross-sectional view of the sample shows that the CsPbBr_3 MC striped films have a thickness of 5 μm , and the ITO patterns are occupied by CsPbBr_3 MCs. The result of AFM measurement is also obtained, which is shown in Fig. S2. The arithmetical mean deviation of R_a (roughness) at two different positions of the device is 776 nm and 875 nm. The morphology of the perovskite is not so planarity; nevertheless, more light compensating contact surface collects more incident light.

Furthermore, the molar ratio of about 1:1:3 (Cs:Pb:Br) confirms the formation of CsPbBr_3 . The X-ray diffraction (XRD) pattern shown in Fig. 1(e) with sharp diffraction peaks verifies that the MC striped films belong to the cubic structure of CsPbBr_3 (JCPDS No. 54-0752).⁴⁰ Figure 1(f) displays the photoluminescence (PL) spectrum of the CsPbBr_3 film, and the main peak is located at 550 nm with the relatively narrow full width at half-maximum (FWHM) of 23.7 nm, which is consistent with previously reported works.^{24,38} All of these results demonstrate that high quality CsPbBr_3 MC striped films are grown on the ITO substrates.

To value the junction between CsPbBr_3 striped films and ITO electrodes, the exponential I - V curves of the obtained device under dark condition were depicted and shown in Fig. 2(a). The dark current (I_D) of the device reveals the rectifying behavior of the Schottky junction. For a Schottky junction, the thermionic emission diffusion theory is chosen to describe the I - V characteristics, and then, I_D can be defined as follows:⁴¹

$$I_D = AA^* T^2 \exp\left(-\frac{\Phi_B}{kT}\right) \exp\left(\frac{qV}{\eta kT}\right), \quad (1)$$

where A is the contact area, A^* is the Richardson constant, Φ_B is the Schottky barrier height, q is the elementary charge, V is the applied bias, η is the ideality factor of 1 here, k is Boltzmann's constant, and

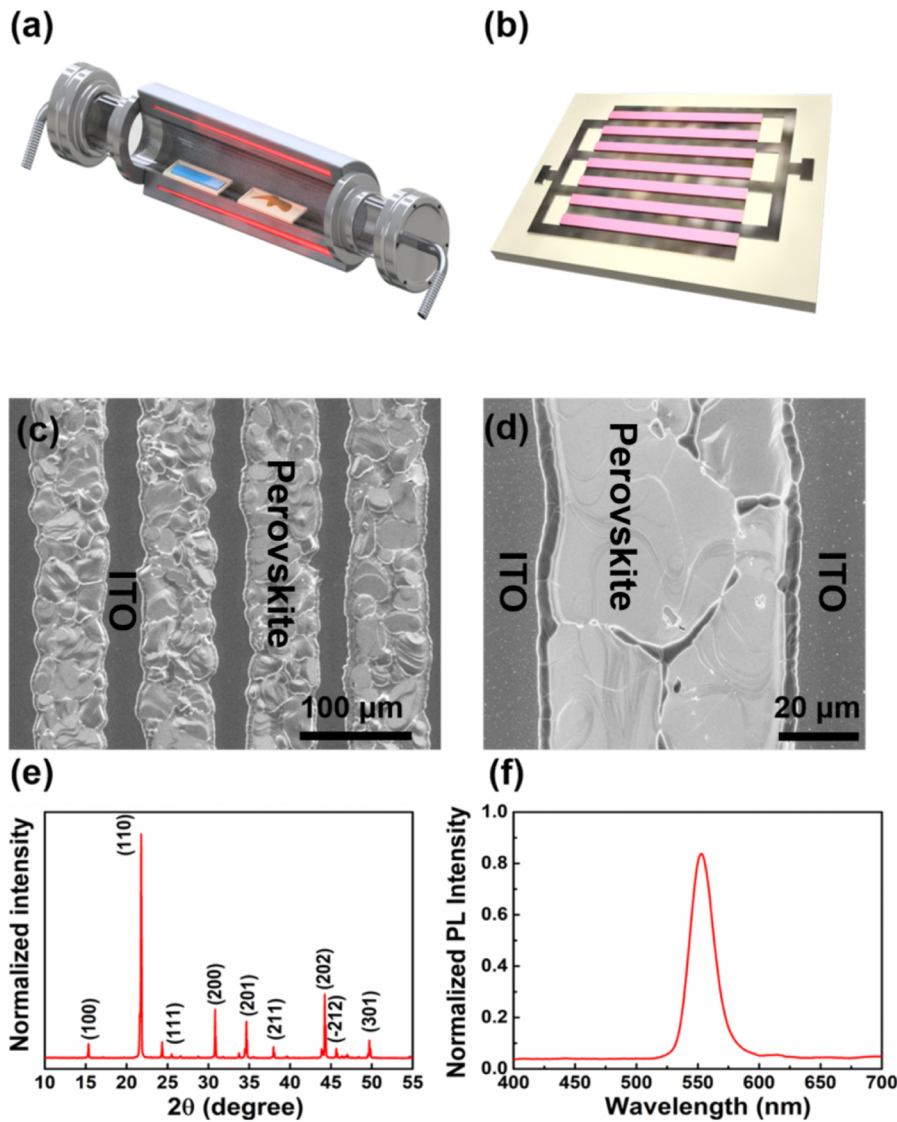


FIG. 1. (a) Schematic of the CsPbBr₃ striped film growth process. (b) Diagrammatic sketch of the device. [(c) and (d)] SEM image of the CsPbBr₃ striped films on the IDL ITO pattern. (e) XRD spectrum indicating the cubic structure of CsPbBr₃. (f) Steady-state PL spectrum ($\lambda_{\text{ex}} = 325 \text{ nm}$).

T is the temperature. From Eq. (1), Φ_B can be calculated by fitting the linear region of the I - V curve [Fig. 2(a)]. The calculated values of Φ_B are about 0.75–0.81 eV (A^* taken as 10 – $100 \text{ A cm}^{-2} \text{ K}^{-2}$) for the ITO/CsPbBr₃ junction. The high Schottky barrier of the device results in the low leak current of a few pico-ampere at 0 V bias. Figure 2(b) displays the I - V characteristics and the energy band diagram of the device, and the threshold voltage of the junction is around 9 V, which is much higher than previously reported values.^{34–36}

After being illuminated by 540 nm light ($92 \mu\text{W}$), the photocurrent (red line) of the device in the range from -15 V to 15 V has increased by 4 orders of magnitude than dark current in Fig. 2(a). To reveal the photoresponse of our detector to the incident optical signal, the responsivity (R) of the device was calculated. R is defined as I_{ph}/L_{light} , where I_{ph} is the photocurrent and L_{light} is the

incident light power. The responsivity under 540 nm incident light shows the exponential increase with the voltage from 0 V to 15 V in Fig. 2(c), which then reaches the highest value of 3.9 A W^{-1} at 15 V. Figure 2c also displays the external quantum efficiency (EQE), which can be calculated from the responsivity with the equation $\eta = Rhc/q\lambda$, where λ is the incident light wavelength and h is Planck's constant. The high EQE implies the existence of high photoconductive gain in the device. The linear dynamic range (LDR) was calculated using the equation $LDR = 20 \log(I_{ph}^*/I_D)$, and as shown in Fig. 2(d) (back line), the value of LDR retains at about 90 dB with bias range from 4 V to 6 V. Also, the detectivity (D^*) is another figure-of-merit for PDs, which describes the weakest detectable signal and can be defined as $D^* = A^{1/2}R/(2qI_D)^{1/2}$, where A is the effective area taken as 4 mm^2 . In our case, as shown in Fig. 2(d) (blue line), the D^* value could reach up to $3.6 \times 10^{12} \text{ Jones}$ ($\text{Jones} = \text{cm Hz}^{1/2} \text{ W}^{-1}$), which

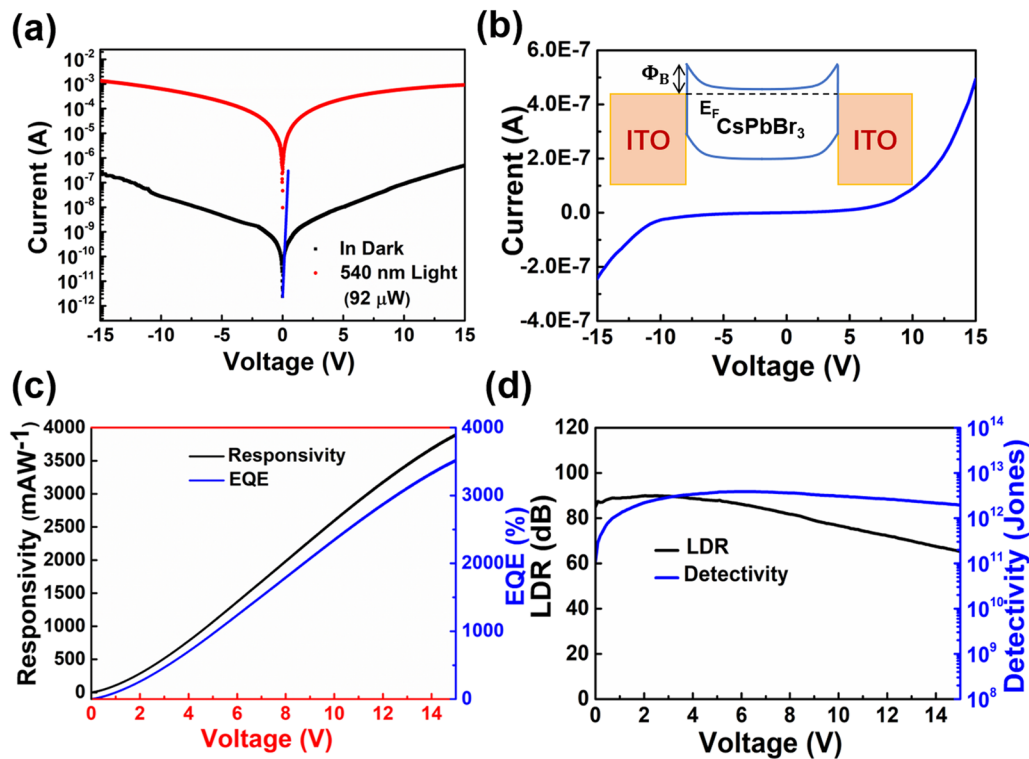


FIG. 2. (a) Current-voltage correlation in dark and under the incident light of 92 μW for as-designed PD and thermionic emission fitting to I - V characteristics for Φ_B calculation. (b) I - V characteristics of the device; the inset shows the energy band diagram of the device. (c) Responsivity and EQE and (d) detectivity and LDR as a function of the bias voltage of the PDs.

demonstrates that the introduction of Schottky barriers provides an effective way to overcome the trade-off between the responsivity and dark current.

The spectral response spectra of the PD were measured from 350 nm to 650 nm under different bias voltages, i.e., 2, 4, 6, and 8 V in Fig. 3(a). The responsivity curves under different bias voltages show the same spectral shape, and the peak is located at 530 nm, which is in accordance with the bandgap of CsPbBr₃ MCs (2.34 eV). The value of EQE and D^* under the light illumination of different wavelengths was calculated and plotted in Fig. S2 (supplementary material). It shows that the curves of both EQE and D^* display the same tendency as responsivity curves. Figure 3(b) presents the successive on/off switching tests of the PD at 4 V bias under the light power ranging from 8 μW to 92 μW , which demonstrates that the photocurrent increases with the increasing illumination power. As shown in Fig. 3(c), it displays the linear relationship between the photocurrent and illumination power. Also, on/off switching tests indicate that the PD has good reproducibility after several response cycles. Under 540 nm light illumination, the responsivity and detectivity increase with the decreasing illumination power, which could reach up to 1.6 AW^{-1} and 1375%, respectively [Fig. (3d)]. Figure S3 (supplementary material) also shows the I - V curves of the PDs in dark and under homogeneous light illumination with different powers.

The response speed is another important parameter of PDs, which reflects their reaction capacity to varying optical signals. Compared with the photoconductive PDs, the photovoltaic PDs with energy barriers usually have faster response speed due to their rapid collection of photon-generated carriers by the built-in electric field. In this work, we used a chopper to turn on/off the 405 nm laser illuminated on the device [shown in Fig. 3(e)]. Figure 3(f) depicts the photoresponse characteristics of the device at high frequency under the bias of 4 V. It can be seen that the device responds to the varying light signal reproducibly and quickly. In addition, the rise (τ_{rise}) time of the dark current from 10% to 90% is 0.22 ms, and the fall (τ_{fall}) time of photocurrent from 90% to 10% is 0.45 ms. The fast photoresponse speed can be attributed to the rapid separation and efficient extraction of photo-induced carriers under the effect of the strong built-in field, which is formed by the Schottky junction between CsPbBr₃ MC films and ITO electrodes. The high performance of our PDs over a wide bias range from -15 V to 15 V is believed to benefit from the high crystal quality of the CsPbBr₃ MC film and the high Schottky barrier height at the perovskite/ITO interface.

It is known that the stability of perovskite-based devices is still a challenging issue. For revealing the stability of our device, the performance of the PD under the temperature of 298 K, 323 K, 348 K, and 373 K were measured under 1 V bias. As shown in Fig. S4

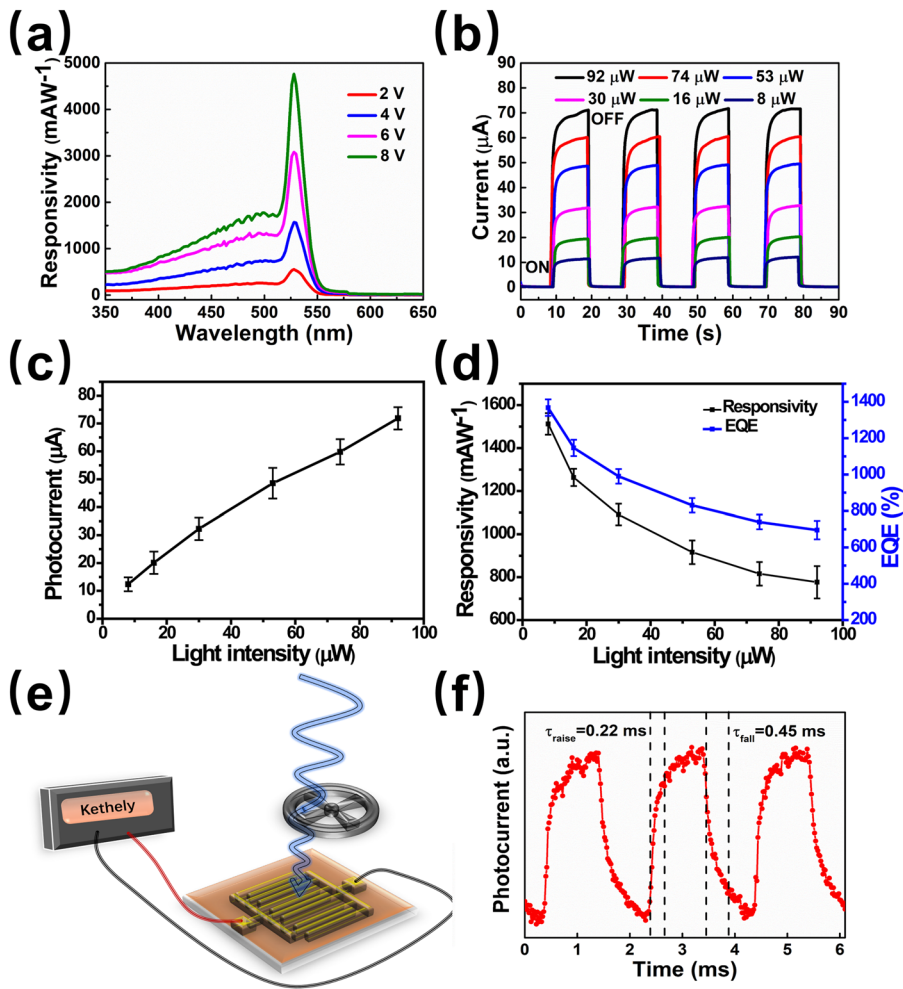


FIG. 3. (a) Spectral responsivity of the PDs. (b) The reproducible on/off switching of the device under illumination of various light intensities at the bias of 4 V. Power-dependent photocurrent (c) and responsivity and EQE (d) under 4 V bias. (e) Schematic of the PD to measure the photoresponse speed. (f) Response of the device to pulsed light irradiation at a frequency of 500 Hz.

(supplementary material), both the photocurrents and dark currents are all increased with increasing temperature. However, the increasing rate of dark current is faster than that of photocurrent, which results in the decay of on/off ratio from 4 orders of magnitude to 2 in Fig. 4(a). For perovskites, the temperature-dependent current

increase can be ascribed to the thermal iron migration.^{40,41} The activated irons will not only enhance the conductivity of material but also weaken the influence of the Schottky barrier effect. Figure 4(b) shows the integrated curves of on/off switching currents under different temperature. It is worth noting that there are spikes on the

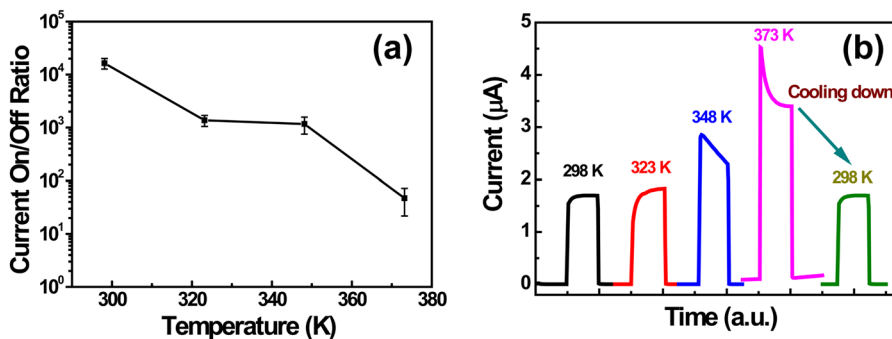


FIG. 4. (a) Temperature-dependent current on/off ratio. (b) On/off switch tests of the device under different temperatures.

curves under the temperature of above 348 K, and the photocurrent reaches to a maximum value when the light is turned on and is then followed by a decay. It may originate from the dipole rearrangement of thermal activated ions.⁴² It is important that our device shows a recoverable performance. After cooling to 298 K, the photocurrent [green curve, Fig. 4(b)] could recover to the initial level. The above studies display that the performance of our device has no tendency to deteriorate under high temperature environments. Few defects, less grain boundaries, and high quality microcrystalline contribute to the enhanced stability of the device. The results give a promising strategy for the application of high performance and stable perovskite-based devices.

In summary, we have demonstrated a direct growth approach of CsPbBr₃ MC films on IDL patterned ITO electrodes by the CVD method. The decent Schottky junctions were obtained at the perovskite/ITO interface. The Schottky barrier height and threshold voltage of the junction were 0.75–0.81 eV and 9 V, which is much higher than previously reported values. The dark current of the back-to-back Schottky junction PD was suppressed with the M-S contacts without a complicated fabrication process. The device exhibited the on/off photocurrent ratio of 10⁴, responsivity of 3.9 AW⁻¹ (at 4 V), detectivity of up to 3.8 × 10¹² Jones, and fast response speed of 0.22 ms (raise time) and 0.45 ms (fall time). In addition, the device presented the enhanced stability, which could retain the performance under high temperature environments. This work not only demonstrates a way to construct high quality Schottky junctions of CsPbBr₃ and electrodes but also offers a promising candidate for stable and high-performance PDs.

See the [supplementary material](#) for the cross-sectional SEM image of CsPbBr₃ MC striped films, spectral responsivity, and detectivity of the PDs with different bias voltages, power-dependent I-V curves of the PDs, and temperature-dependent currents.

This work was supported by the National Natural Science Foundation of China under Grant Nos. 11874351, 11874352, and 61805237 and the Research Foundation of Jilin province under Grant No. 20180519004JH.

REFERENCES

- X. Gao, Y. Cui, R. M. Levenson, L. W. K. Chung, and S. Nie, *Nat. Biotechnol.* **22**, 969 (2010).
- S. K. Jain, S. Krishna, N. Aggarwal, R. Kumar, A. Gundimeda, S. C. Husale, V. Gupta, and G. Gupta, *J. Electron. Mater.* **47**, 6086 (2018).
- B. Zhao, F. Wang, H. Chen, Y. Wang, M. Jiang, X. Fang, and D. Zhao, *Nano Lett.* **15**, 3988–3993 (2015).
- B. Jalali and S. Fathpour, *J. Lightwave Technol.* **24**, 4600 (2006).
- A. Poglitsch, C. Wealkens, N. Geis, H. Feuchtgruber, B. Vandenbussche, L. Rodriguez, O. Krause, E. Renotte *et al.*, *Astron. Astrophys.* **518**, L2 (2010).
- H. Zhu, Y. Fu, F. Meng, X. Wu, Z. Gong, Q. Ding, M. V. Gustafsson, M. Tuan Trinh, S. Jin, and X.-Y. Zhu, *Nat. Mater.* **14**, 636–642 (2015).
- A. Fu and P. Yang, *Nat. Mater.* **14**, 557–558 (2015).
- Z.-K. Tan, R. S. Moghaddam, M. L. Lai, P. Docampo, R. Higler, F. Deschler, M. Price, A. Sadhanala, L. M. Pazos, D. Credgington, F. Hanusch, T. Bein, H. J. Snaith, and R. H. Friend, *Nat. Nanotechnol.* **9**, 687 (2014).
- Y.-H. Kim, H. Cho, J. H. Heo, T.-S. Kim, N. S. Myoung, C.-L. Lee, S. H. Im, and T.-W. Lee, *Adv. Mater.* **27**, 1248–1254 (2015).
- H. Cho, S.-H. Jeong, M.-H. Park, Y.-H. Kim, C. Wolf, C.-L. Lee, J. H. Heo, A. Sadhanala, N. Myoung, S. Yoo, S. H. Im, R. H. Friend, and T.-W. Lee, *Science* **350**, 1222–1225 (2015).
- Y. Liu, Y. Zhang, Z. Yang, H. Ye, J. Feng, Z. Xu, X. Zhang, R. Munir, J. Liu, P. Zuo, Q. Li, M. Hu, L. Meng, K. Wang, D.-M. Smilgies, G. Zhao, H. Xu, Z. Yang, A. Amassian, J. Li, K. Zhao, and S. (Frank)Liu, *Nat. Commun.* **9**, 5302 (2018).
- L. Dou, Y. Yang, J. You, Z. Hong, W.-H. Chang, G. Li, and Y. Yang, *Nat. Commun.* **5**, 5404 (2014).
- H. Wei, Y. Fang, P. Mulligan, W. Chuirazzi, H.-H. Fang, C. Wang, B. R. Ecker, Y. Gao, M. A. Loi, L. Cao, and J. Huang, *Nat. Photonics* **10**, 333 (2016).
- R. Dong, Y. Fang, J. Chae, J. Dai, Z. Xiao, Q. Dong, Y. Yuan, A. Centrone, X. Zeng, and J. Huang, *Adv. Mater.* **27**, 1912–1918 (2015).
- N. J. Jeon, J. H. Noh, W. S. Yang, Y. C. Kim, S. Ryu, J. Seo, and S. Il Seo, *Nature* **517**, 476–480 (2015).
- W. Nie, H. Tsai, R. Asadpour, J.-C. Blancon, A. J. Neukirch, G. Gupta, J. J. Crochet, M. Chhowalla, S. Tretiak, M. A. Alam, H.-L. Wang, and A. D. Mohite, *Science* **347**, 522–525 (2015).
- K. Domanski, E. A. Alharbi, A. Hagfeldt, M. Grazel, and W. Tress, *Nat. Energy* **3**, 61–67 (2018).
- M. Kulbak, S. Gupta, N. Kedem, I. Levine, T. Bendikov, G. Hodes, and D. Cahen, *J. Phys. Chem. Lett.* **7**, 167–172 (2016).
- L. Protesescu, S. Yakunin, M. I. Bodnarchuk, F. Krieg, R. Caputo, C. H. Hendon, R. X. Yang, A. Walsh, and M. V. Kovalenko, *Nano Lett.* **15**, 3692–3696 (2015).
- M. Shoaib, X. Zhang, X. Wang, H. Zhou, T. Xu, X. Wang, X. Hu, H. Liu, X. Fan, W. Zheng, T. Yang, S. Yang, Q. Zhang, X. Zhu, L. Sun, and A. Pan, *J. Am. Chem. Soc.* **139**, 15592–15595 (2017).
- J. Song, L. Xu, J. Li, J. Xue, Y. Dong, X. Li, and H. Zeng, *Adv. Mater.* **28**, 4861–4869 (2016).
- X. Liu, D. Yu, F. Cao, X. Li, J. Ji, J. Chen, X. Song, and H. Zeng, *Small* **13**, 1700364 (2017).
- Y. Li, Z.-F. Shi, S. Li, L.-Z. Lei, H.-F. Ji, D. Wu, T.-T. Xu, Y.-T. Tian, and X.-J. Li, *J. Mater. Chem. C* **5**, 8355–8360 (2017).
- M. I. Saidaminov, M. A. Haque, J. Almutlaq, S. Sarmah, X.-H. Miao, R. Begum, A. A. Zhumekenov, I. Dursun, N. Cho, B. Murali, O. F. Mohammed, T. Wu, and O. M. Bakr, *Adv. Opt. Mater.* **5**, 1600704 (2017).
- J. Song, Q. Cui, J. Li, J. Xu, Y. Wang, L. Xu, J. Xue, Y. Dong, T. Tian, H. Sun, and H. Zeng, *Adv. Opt. Mater.* **5**, 1700157 (2017).
- Y. H. Dong, Y. Gu, Y. S. Zou, J. Z. Song, L. M. Xu *et al.*, *Small* **12**, 5622–5632 (2016).
- L. Zhou, K. Yu, F. Yang, H. Cong, N. Wang *et al.*, *J. Mater. Chem. C* **5**, 6224–6233 (2017).
- X. F. Song, X. H. Liu, D. J. Yu, C. X. Huo, J. P. Ji *et al.*, *ACS Appl. Mater. Interfaces* **10**(3), 2801–2809 (2018).
- B. Yang, F. Y. Zhang, J. S. Chen, S. Q. Yang, X. S. Xia *et al.*, *Adv. Mater.* **29**, 1703758 (2017).
- F. Cao, D. J. Yu, X. M. Li, Y. Zhu, Z. G. Sun *et al.*, *J. Mater. Chem. C* **5**, 7441–7445 (2017).
- H. Zhou, J. P. Zeng, Z. N. Song, C. R. Grice, C. Chen *et al.*, *J. Phys. Chem. Lett.* **9**, 2043–2048 (2018).
- K. Skucha, Z. Fan, K. Jeon, A. Javey, and B. Boser, *Sens. Actuators, B* **145**, 232–238 (2010).
- J. Svensson and E. E. B. Campbell, *J. Appl. Phys.* **110**, 111101 (2011).
- C. Park, J. Lee, H.-M. So, and W. S. Chang, *J. Mater. Chem. C* **3**, 2737 (2015).
- M. Zhang, L. L. Brooks, N. Chartuprayoon, W. Bosze, Y. Choa, and N. V. Myung, *ACS Appl. Mater. Interfaces* **6**, 319–326 (2014).
- P. A. Shaikh, D. Shi, J. Ramon, D. Retamal, A. D. Sheikh, M. A. Haque, C.-F. Kang, J.-H. He, O. M. Bakr, and T. Wu, *J. Mater. Chem. C* **4**, 8304 (2016).
- X. Guan, W. Hu, M. A. Haque, N. Wei, Z. Liu, A. Chen, and T. Wu, *Adv. Funct. Mater.* **28**, 1704665 (2018).
- P. Gui, Z. Chen, B. Li, F. Yao, X. Zheng, Q. Lin, and G. Fang, *ACS Photonics* **5**, 2113–2119 (2018).

³⁹C. Tian, F. Wang, Y. Wang, Z. Yang, X. Chen, J. Mei, H. Liu, and D. Zhao, [ACS Appl. Mater. Interfaces](#) **11**, 15804–15812 (2019).

⁴⁰Y. Li, Z. Shi, L. Lei, F. Zhang, Z. Ma, D. Wu, T. Xu, Y. Tian, Y. Zhang, G. Du, C. Shan, and X. Li, [Chem. Mater.](#) **30**, 6744–6755 (2018).

⁴¹B. Roul, M. K. Rajpalke, T. N. Bhat, M. Kumar, N. Sinha, A. T. Kalghatgi, and S. B. Krupanidhi, [J. Appl. Phys.](#) **109**, 044502 (2011).

⁴²F. Wang, J. Mei, Y. Wang, L. Zhang, and D. Zhao, [ACS Appl. Mater. Interfaces](#) **8**, 2840–2846 (2016).